Geophysical Research Letters

RESEARCH LETTER
10.1029/2021GL096683

# Understanding Differences in North Atlantic Poleward Ocean Heat Transport and Its Variability in Global Climate Models

**Erica Madonna**[1,2] **and Anne Britt Sandø**[2,3]

[1]Geophysical Institute, University of Bergen, Bergen, Norway, [2]Bjerknes Centre for Climate Research, Bergen, Norway, [3]Institute of Marine Research, Bergen, Norway

**Abstract** The ocean heat transport from the North Atlantic to the Barents Sea impacts the sea ice extent and the energy budget of the Arctic. The analyzed climate models from the fifth (CMIP5) and sixth Coupled Model Intercomparison Project phase 6 (CMIP6) phases of the Coupled Model Intercomparison Project show large intermodel differences in the ocean heat transport with biases of several Terawatts at the Iceland-Scotland Ridge and Barents Sea Opening (BSO). While both model generations show a large spread in mean volume transports, in CMIP6 temperatures are more homogeneous and realistic, yielding heat transports closer to observations. On all time scales, changes in heat transport reflect changes in volume transport, while temperature changes affect the heat transport variability on longer time scales, especially at the BSO. The temporal variability of heat and volume transports is linked to wind forcing south of Iceland and along the Norwegian coast in all models but has different magnitudes.

**Plain Language Summary** The ocean currents transport heat poleward from the North Atlantic to the Barents Sea and influence the formation and melting of Arctic sea ice. Climate models from the fifth (CMIP5) and sixth Coupled Model Intercomparison Project phase 6 (CMIP6) phases of the Coupled Model Intercomparison Project show large differences in the amount of transported heat at the Iceland-Scotland Ridge and Barents Sea Opening (BSO). Compared to CMIP5 models, the analyzed CMIP6 models show improved mean temperatures at both locations, resulting in ocean heat transport closer to observations. The strength of the ocean currents controls much of the variability of the heat transport, but the water temperature is also important at the BSO. The temporal variability of the heat and volume transport is linked to wind forcing south of Iceland and along the Norwegian coast in all models. However, there are differences in the magnitude of the ocean response.

E. Madonna and A. B. Sandø contributed equally to this work.

**Key Points:**

- Improved water temperature in the analyzed Coupled Model Intercomparison Project phase 6 climate models yields mean ocean heat transports closer to observations and less inter-model spread
- Temporal changes in ocean heat transport reflect volume transport changes, while temperature matters on longer time scales at the Barents Sea Opening
- Wind variability south of Iceland affects the variability of the volume transport in most models with different regression magnitudes

**Supporting Information:**

Supporting Information may be found in the online version of this article.

**Correspondence to:**

E. Madonna,
erica.madonna@uib.no

**Citation:**

Madonna, E., & Sandø, A. B. (2022). Understanding differences in North Atlantic poleward ocean heat transport and its variability in global climate models. *Geophysical Research Letters*, *49*, e2021GL096683. https://doi.org/10.1029/2021GL096683

Received 19 OCT 2021
Accepted 1 DEC 2021



## 1. Introduction

Ocean currents are key components of the climate system, as they transport energy poleward from the tropics to high-latitudes. The poleward energy transport may be altered by anthropogenic climate change (Burgard & Notz, 2017; Huang et al., 2017; Nummelin et al., 2017; Spielhagen et al., 2011), leading to profound impacts on the fragile Arctic system, such as changes in the sea ice cover, the distribution of species, and economic activities (ACIA, Arctic Climate Impact Assessment, 2004). Changes in sea ice cover, in turn, can influence the albedo and the heat fluxes between the ocean and atmosphere (Ikeda, 1990; Screen & Simmonds, 2010; Serreze et al., 2009; Smedsrud et al., 2013; Winton, 2006), further amplifying the warming of the Arctic (Serreze & Barry, 2011).

To understand the future evolution of the Arctic system we use climate models, but these struggle to represent the present sea ice variability and the observed long-term trends, in particular in the Barents Sea (Li et al., 2017). Trends in sea ice cover from most models that contributed to the Coupled Model Intercomparison Project Phase 5 (CMIP5) are less negative than the observed trends (Li et al., 2017; Stroeve et al., 2012). A distinct improvement in the representation of the sea ice volume and extent is obtained in Coupled Model Intercomparison Project phase 6 (CMIP6) (Davy & Outten, 2020; Notz and SIMIP Community, 2020), but numerous model biases persist, including too cold conditions in winter.

The ocean heat transport (OHT) into the Arctic is crucial for determining the sea ice variability in the Barents Sea and the Arctic Ocean (Årthun et al., 2012, 2019; Onarheim et al., 2015; Sandø et al., 2014; Docquier et al., 2021). Warm water from the Atlantic basin circulates through the Iceland-Scotland Ridge (ISR) transporting ~231 ± 43 TW of heat and moves poleward along the Norwegian coast as Norwegian Atlantic Current (Skagseth et al., 2008). Part of this warm current continues through the Barents Sea Opening (BSO) with ~75 ± 20 TW of heat, reaching the Barents Sea (Figure 1a) and contributes to sea ice melting ( Årthun et al., 2012; Smedsrud

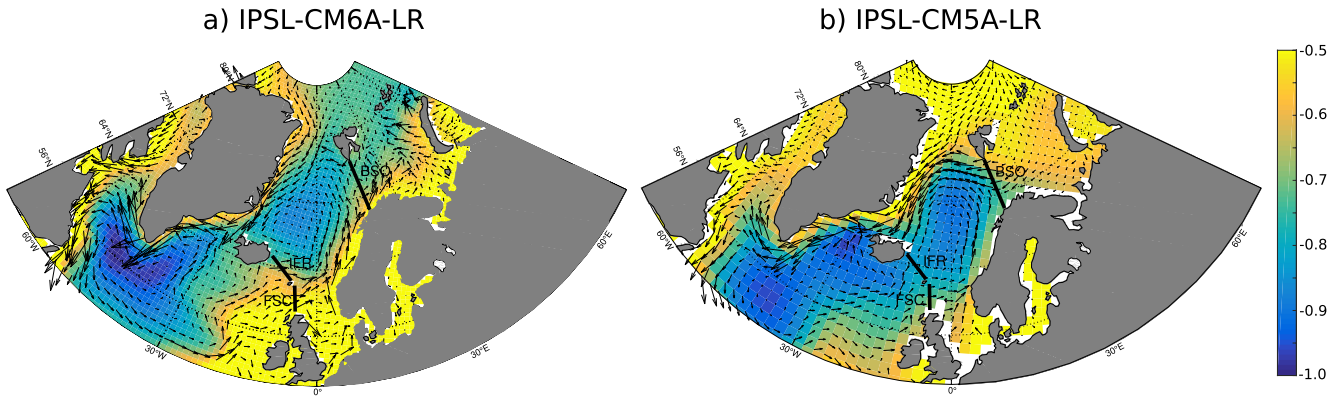


**Figure 1.** Sea level height (*zos*, color, in m) and surface velocities (arrows) for the (a) IPSL-CM6A-LR Coupled Model Intercomparison Project phase 6 and (b) IPSL-CM5A-LR (CMIP5) model. The black lines denote the location of the Iceland-Scotland Ridge [ISR, i.e., the sum of the Iceland-Faroe Ridge (IFR) and the Faroe-Shetland Channel (FSC)] and the Barents Sea Opening (BSO) used for the calculation of OHT, OVT, and temperature. These two models were chosen to exemplify differences in the sign of the OVT at the BSO.

et al., 2013). The northwards transport of warm water close to the surface accounts for most of the total OHT (Boccaletti et al., 2005; Hátún, Sandø, Drange, Hansen, & Valdimarsson, 2005).

The OHT depends on the amount of transported water (i.e., the ocean volume transport, OVT) and its temperature (Buckley & Marshall, 2016; Orvik & Skagseth, 2005). The same OHT can result from the transport of a large volume of relatively cold water, or a small volume of relatively warm water. The relative importance of these two components (OVT and temperature) for the OHT depends on the considered time scale and location. Observations at the BSO indicate that the OVT dominates the OHT signal on shorter time scales, while on longer time scales water temperature is also important (Orvik & Skagseth, 2005). At the Fram Strait, modeled long-term OHT variability is dominated by variations in temperature (Muilwijk et al., 2018). Therefore, to better understand why climate models have so different OHT it is key to consider both components of the OHT at different time scales.

Finally, OHT is linked to ocean currents that are forced by the atmosphere (Lien et al., 2017; Orvik & Skagseth, 2003; Richter et al., 2009; Sandø et al., 2012; Sandø & Furevik, 2008; Serra et al., 2010), so OHT differences in models could also result from differences in wind forcing (Muilwijk et al., 2018, 2019). Since the representation of the jet stream and the storm tracks over the North Atlantic is often too zonal in CMIP5 and CMIP6 (Harvey et al., 2020; Oudar et al., 2020; Priestley et al., 2020; Zappa et al., 2014), these biases can have implications for the representation of the wind stress curl and ocean circulation.

To understand present and future changes in the Arctic regions, it is crucial to investigate what controls the OHT and its variability, as this has an impact on the poleward energy transport and sea ice extent. In this study, we consider the OHT into the Nordic and Barents Seas across 15 CMIP5 and 9 CMIP6 models. We focus on the ISR and BSO only, on the one hand, because the Fram Strait transports are strongly influenced by eddy-driven variability (Muilwijk et al., 2018), which cannot be realistically reproduced in the low-resolution global models. On the other hand, to compare models and observations, continuous measurements are needed and are available for these two sections for more than two decades. The goal of the study is to understand which factors account for the intermodel differences in the OHT mean state and variability. We consider the water temperature and OVT, as well as the atmospheric wind forcing, which is expected to influence the OVT.

## 2. Data and Method

### 2.1. Observations and Reanalyses

The observation-based numbers are combinations of different observational time series and estimates. The net OHT and OVT at the BSO consist of combined estimates for different water masses based on the inflow of Atlantic Water (Ingvaldsen et al., 2004; Skagseth, 2008) and Norwegian Coastal Current water (Skagseth et al., 2011) from the Norwegian Marine Data Center (NMDC, 2020) from 1998 to 2016. The OHT and OVT at the ISR are based on the inflow of Atlantic Water (Berx et al., 2013; Hansen & Østerhus, 2000) and outflow of deep waters (Hansen & Østerhus, 2000, 2007) at the Iceland-Faroe Ridge (IFR) and Faroe-Shetland Channel (FSC) from

AtlantOS (OceanSITES, 2020) from 1993. These estimates are available at a monthly resolution. Time series of annual temperatures representing northward-flowing Atlantic Water (i.e., the upper 200 meters) are taken from the ICES Report on Ocean Climate (ICES, 2020). For comparison with model data, we use values only until 2005, and the climatological means are reported in Table S1.

For the atmospheric forcing, we use the zonal wind (U) at 850 hPa from the twentieth-century atmospheric reanalysis (ERA-20C) of the European Center for Medium-Range Weather Forecasts (Poli et al., 2016) available for 1900–2010.

### 2.2. CMIP5 and CMIP6 Model Data

Modeled data from CMIP5 (Taylor et al., 2012) and CMIP6 (Eyring et al., 2016) is downloaded from the Earth System Grid Federation (ESGF; Cinquini et al., 2014). The analysis is based on monthly outputs over the periods 1850–2005 (or 1986–2005 when comparing to observations) with ensemble members r1i1p1 and r1i1p1f1 from 15 CMIP5 and 9 CMIP6 models, respectively. Only models that provide variables for both heat (*hfx*, *hfy*) and mass (*umo*, *vmo*) transports per month are included. Thereby, *hfx* and *hfy* (*umo* and *vmo*) contain all contributions to x- and y-ward heat (mass) transport from resolved and parameterized processes. Volume transports are calculated from mass transports assuming a density of water of 1000 kg $m^{-3}$. This assumption can lead to a slight (< 3%) overestimation of OVT but it does not affect its variability (not shown). In addition, we consider monthly ocean temperatures *(thetao)* at 100 m depth and zonal wind (U) at 850 hPa. Sea level height (*zos*) and ocean surface velocity (*uo* and *vo* components) are used to illustrate circulation differences in Figure 1.

### 2.3. Calculation of the Ocean Heat and Volume Transports

The OHT through a section S depends on the amount of transported water and its temperature. Following Orvik and Skagseth (2005) it is defined as

$$OHT = \int_S c_p \rho \mathbf{v} T \, dS \tag{1}$$

where, $c_p$ is the specific heat capacity of water, $\rho$ the density of seawater, $\mathbf{v}$ the velocity of the water perpendicular to section $S$, and $T$ the temperature of the water relative to a reference temperature of 0°C. The term $\int_S \mathbf{v} dS$ represents the OVT.

We calculate monthly OHT and OVT from the model outputs, and consider two sections shown in Figure 1: the Iceland-Scotland Ridge (ISR), which encompasses the Iceland-Faroe Ridge and the Faroe-Scotland Channel, and the BSO, from southern Svalbard to the Norwegian coast. For each section, we first find grid indices that are closest to specific longitude and latitude positions at each end of the section. We also check that the endpoints are on land as the resolution and the corresponding bathymetry differ from model to model. Thereafter, we find the grid indices and corresponding $x$ and $y$ transport components for each grid cell along a line between the two endpoints to calculate the total OHT and OVT across the considered sections.

For each model, we use the temperature at 100 m depth as an estimation for the Atlantic water core temperature, and calculate temperatures along the same sections as for OHT and OVT.

### 2.4. Mean Properties, Seasonal Cycle, Decadal Variability

The mean properties are calculated for the period 1986–2005 for both CMIP5 and CMIP6 models to cover a similar period as in the observational estimates. The amplitude of the seasonal cycle is defined as the difference between the lowest and the highest monthly mean values of the considered time series. We also estimate the range of decadal variability by computing a set of 10-year means for different periods using the 150 available years (starting with 1996–2005 going backward, i.e., 1986–1995, 1976–1985. 1856–1865, for a total of 15 periods). We refer to "decadal variability" as the range between the lowest and highest value.

Lag-correlations and regressions are calculated using the period 1850–2005, allowing for a long time series. The regressions of zonal wind at every grid point on the different time series are standardized (regression units are expressed as m $s^{-1}$ per standard deviation of OVT/OHT), and the seasonal cycle and the long-term linear trend have been removed from all time series.

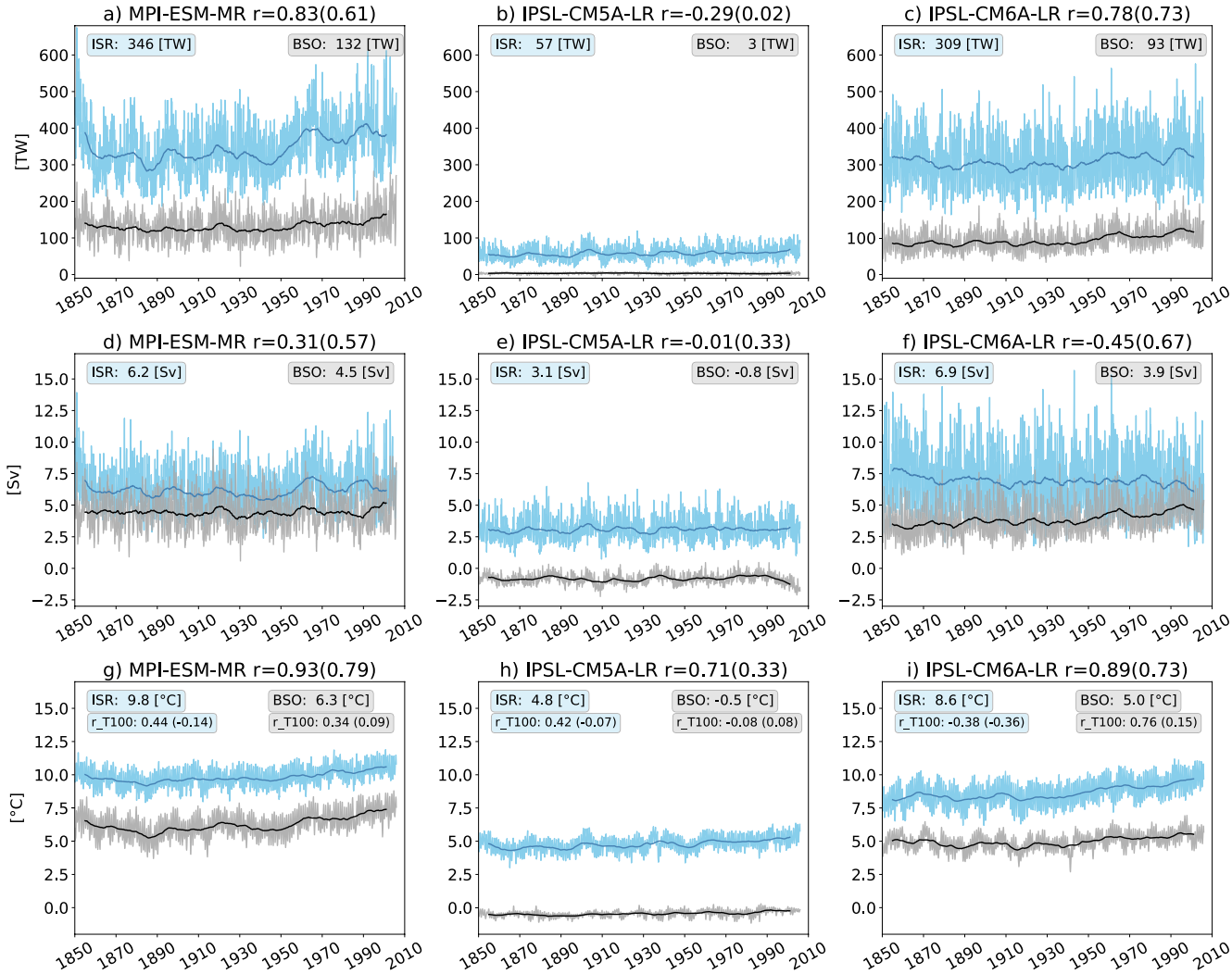


**Figure 2.** Time series of ocean heat transport (a–c, OHT in TW), ocean volume transport (d–f, OVT in Sv), and water temperatures at 100 m (g–i, T100 in °C) for three different models (CMIP5: MPI-ESM-MR, IPSL-CM5A-LR, Coupled Model Intercomparison Project phase 6: IPSL-CM6A-LR). Blue colors show the values for the ISR (IFR and FSC), while gray colors show values for the Barents Sea Opening (BSO). Climatological (1850–2005) values of OHT, OVT, and T100 for the ISR and BSO are shown in the corners of each plot. Thin lines show monthly means and thick lines show decadal means (i.e., the 10-year running means). Correlations (*r*) between the decadal means time series at the two locations (thick lines) are shown at the top of each plot, while correlations using monthly means (thin lines) are shown in brackets. In addition, correlations between decadal temperature and OVT (r_T100) at the ISR (blue) and BSO (gray) are displayed in (g)–(i), and in brackets using monthly data.

## 3. Results

### 3.1. Ocean Mean State and Variability

The mean OHT and its variability at different time scales are differently represented in CMIP models. Figures 2a–2c show the monthly time series of OHT (thin lines) for three different models (cf. Figure S1 for all models). While the MPI-ESM-MR and IPSL-CM6A-LR models have comparable magnitudes of mean OHT at the ISR (values of 346 and 309 TW, respectively, in blue) and BSO (132 and 93 TW, respectively, in gray), the IPSL-CM5A-LR model has much lower values at both locations (57 and 3 TW). On decadal time scales (i.e., applying a running mean of 10 years, thick lines) the models' variability reveals remarkable differences; for example, the MPI-ESM-MR model shows large fluctuations and an increase in OHT between 1940 and 1970 that is not visible in the other models in any periods. The co-variability on decadal (monthly, in brackets) time scales between OHT at the ISR and BSO is for most models positive (cf. Figures 2a–2c with Figure S1) but varies largely in strength.

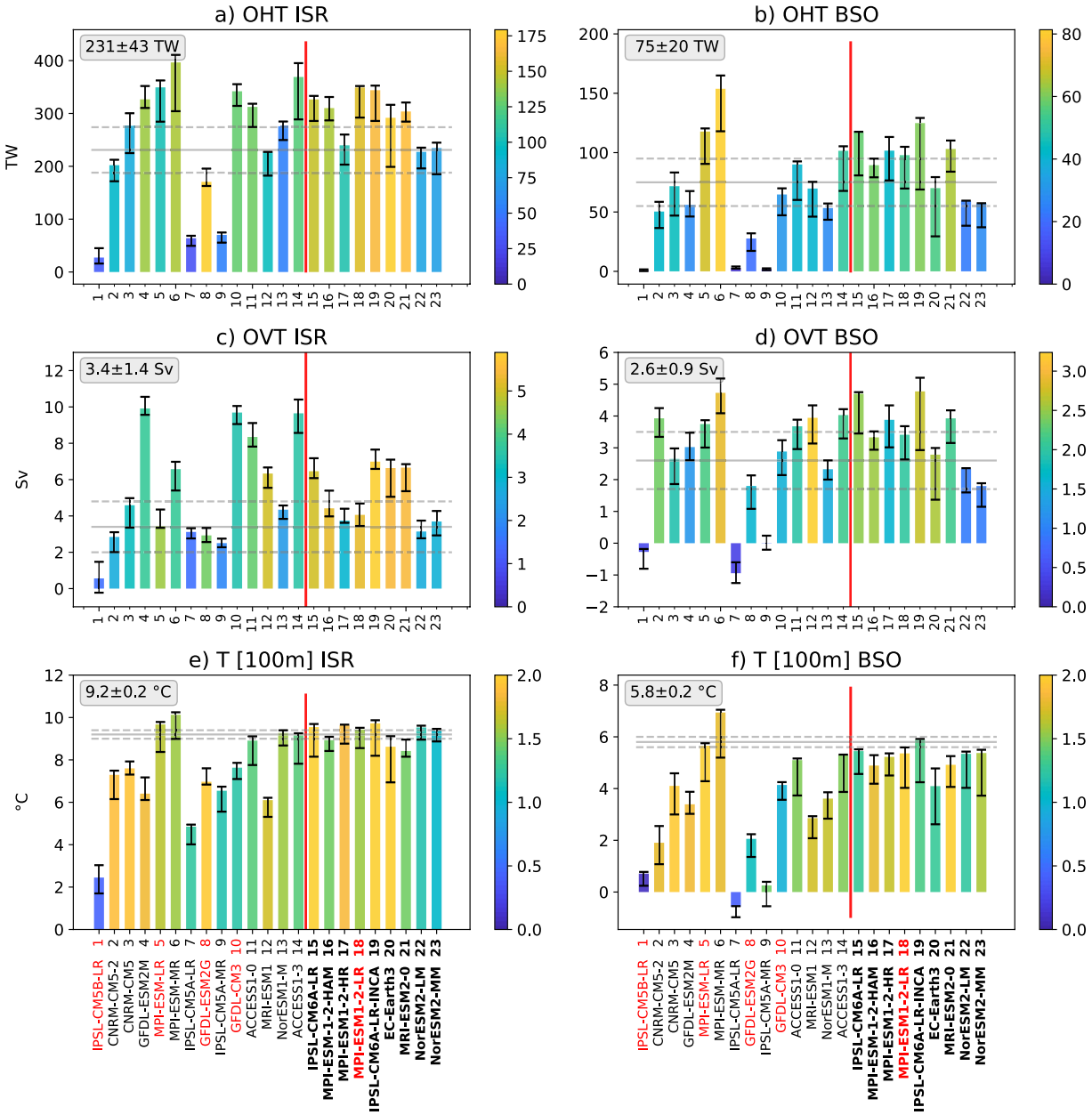


**Figure 3.** Ocean heat transport (a and b, OHT, in TW), ocean volume transport (c and d, OVT, in Sv) and water temperature at 100 m (e-f, T[100m], in °C) at the ISR (left) and Barents Sea Opening (BSO) (right) for different CMIP5/Coupled Model Intercomparison Project phase 6 (CMIP6) models. Bar height shows the mean values for the period 1986–2005, black segments the range of decadal variability (i.e., the minimum and maximum of 10-year means, for the whole period 1850–2005), and colors the amplitude of the seasonal cycle (i.e., the difference between the largest and smallest monthly mean values). CMIP5 (CMIP6, in bold) models are displayed left (right) from the red line and are arranged based on wind speed (from low to high) in the box south of Iceland (cf. Table S1 and Figure 5). Red labels indicate models with a low ocean resolution (≤256 × 220 points). Gray horizontal solid (dashed) lines show the mean observed estimates (standard deviations) described in Section 2.1 and their values are reported at the corner of each plot. CMCC-ESM is not shown due to unrealistically large value of OHT at the ISR.

Large differences are also evident in the seasonal cycle and decadal variability of OHT across CMIP models. Figure 3 (and Table S1) summarizes the mean properties (bar height), and the seasonal cycle (color shading) for 1986–2005, and the decadal variability (black segments) for 1850–2005 for all considered models, except CMCC-CESM, which is not displayed due to the unrealistic large values of OHT at the ISR. The estimates from observations are shown as gray horizontal lines and are reported in the corner of each panel. There is a large spread across models, where the OHT at the ISR (Figure 3a) spans from 30 to 400 TW. Compared to the observed OHT of 231 TW, several models overestimate the OHT by almost 100 TW. This overestimation is still

present if we take into account decadal variability (black segments). The models also have very different seasonal cycles that vary from practically 0 to more than 150 TW. Large differences in the OHT climatologies (ranging from 0 to 120 TW), decadal variability (0–50 TW), and seasonal cycles (0–80 TW) are also observed at the BSO (Figure 3b). Positive and negative biases of OHT at the BSO are observed for both CMIP generations. However, taking into account the decadal variability, the OHT for the considered CMIP6 models falls within the observed range.

Observations show that the ratio between the OHT at the ISR and the BSO is about 3 (Table S1). This ratio is for most models (17 out of 24) higher than 3.5, meaning that most models lose more heat on their way northward than observed. Hence not all models with positive OHT biases at the ISR also have excessive OHT at the BSO. For example, the GFDL-CM3 and the EC-Earth models have a positive bias in OHT at the ISR and a ratio of 5.3 and 4.2, respectively, but show OHT values within the observed range at the BSO.

Since the volume of transported water, together with the water temperature, contribute to the OHT (Equation 1), we want to examine whether there is already a large intermodel spread in the OVT. At the ISR the OVT ranges from less than 1 to 10 Sv, while at the BSO it ranges from −1 Sv (i.e., a net transport of water out from the Barents Sea) to ∼5 Sv (Figures 3c and 3d and Table S1). About half of the models simulate an OVT within the observed range at the ISR, but there are several models that largely overestimate the flow. Most models yield OVT values close to the observed range at the BSO, especially if decadal variability is taken into account (black segments, Figures 2d–2f and Figure S2). For both sections, a diversity of OVT seasonality ranges are visible.

Differences in the mean temperature of the Atlantic water (i.e., at 100 m) can also lead to discrepancies in the mean OHT. Among the analyzed models, CMIP6 models have temperatures close to observations at the ISR (∼9°C) and BSO (∼6°C), while CMIP5 models show mostly cold biases at both sections (Figures 3e and 3f). The decadal variation of water temperatures is comparable between models (see also Figures 2g–2i and S3). The seasonal changes of the water temperature at 100 m are for most models and sections in the order of magnitudes of a few degrees.

### 3.2. Lag Correlation of OHT, OVT, and Temperatures

To investigate how OHT is linked to OVT and temperatures (at 100 m) at different time scales, time series for both sections have been correlated with and without running mean (rm) filters. The non-filtered time series (rm = 1) represent the monthly variability, while the time series filtered by a running mean of 48 months (rm = 48) represent multi-annual variability. The correlations are performed at different lags, with negative lags defined such that OHT anomalies lead OVT/temperature anomalies.

The OVT dominates the OHT on monthly time scales at both sections (Figures 4a and 4b, black lines), with correlations close to 1 at lag 0. Compared to monthly time scales, the correlation between temperatures and OHT increases at all lags on longer time scales (multi-annual, Figures 4c and 4d, gray lines). The multi-annual correlations of OHT with OVT and temperature are similar at the BSO, while OHT shows lower correlations with temperature at the ISR (gray line). The correlation between OHT and OVT maximizes at lag 0, while the correlation between OHT and temperature maximizes at negative lags, especially on monthly time scales (Figures 4a and 4b), suggesting that the OHT leads temperature changes by some months. These conclusions hold for both CMIP5 and CMIP6 models (Figures S4 and S5, in blue and orange, respectively), even though there is a large spread in the strength of the correlations.

### 3.3. Atmospheric Mean State and Variability

The large differences in OVT could be linked to differences in wind forcing. We first regress for each model zonal wind at 850 hPa on the OVT at each section and calculate the multi-model mean of the regressions (Figure 5) to identify the region where winds have the strongest influence on OVT. The jet stream location over the North Atlantic (green contours in Figure 5 and S6) is relatively similar in most models, which compared to observations is too zonal, strong, and extending toward Europe, a typical bias of climate models (i.e., Harvey et al., 2020; Oudar et al., 2020). The regression patterns indicate that when the zonal wind is particularly strong on the poleward side of the jet south of Iceland (positive regression values in the black box, Figure 5a),

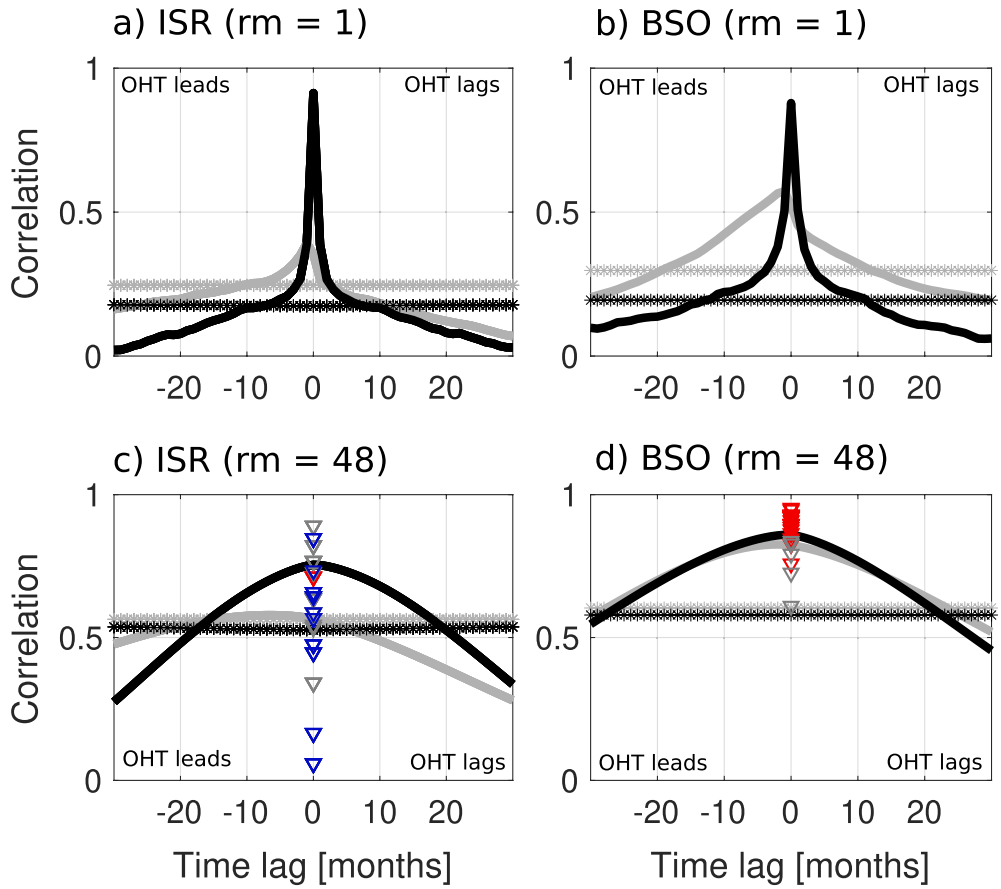


**Figure 4.** Multi-model mean lag correlations for the CMIP5/6 models (without the IPSL-CM5 model versions) between OHT and OVT (black) and between OHT and 100 m temperatures (gray) without running mean filter (rm = 1) at the (a) ISR and (b) Barents Sea Opening (BSO), and (c) and (d) with a running mean filter of 48 months (rm = 48) applied on each time series before correlation. Lag-correlations for each single model are shown in Figures S4 and S5. Triangles in (c) and (d) show the correlation between temperature and OHT for each model at lag 0 and the colors indicate the correlations between temperature and OVT; red for strong positive correlations ($r > 0.5$), gray for weak positive correlations ($0 < r < 0.5$) and blue for negative correlations ($r < 0$). The significance levels (horizontal *) are based on the method described in Chelton (1983). Negative lags mean that OHT leads OVT/temperatures changes.

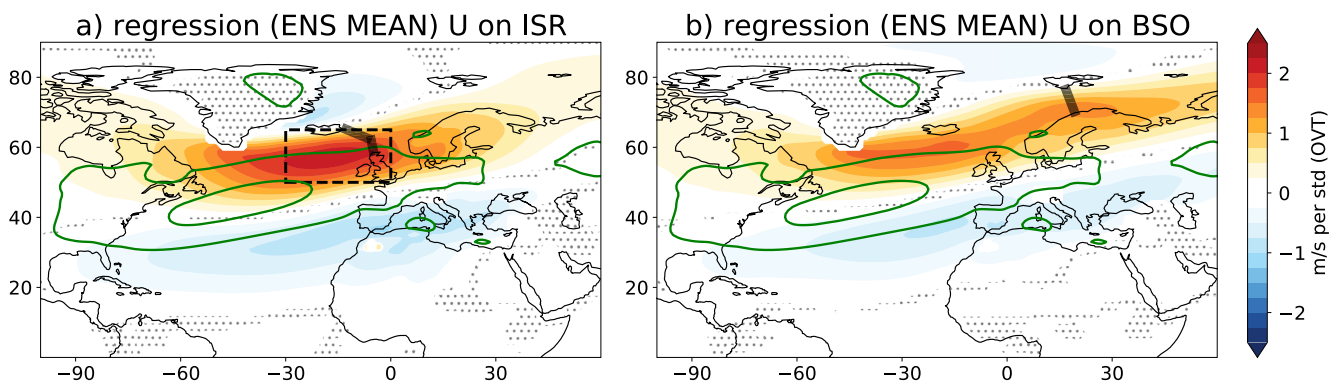


**Figure 5.** Multi-model mean regression of zonal wind (U) at 850 hPa on ocean volume transport (OVT) through the (a) ISR and (b) Barents Sea Opening (BSO) (units: m $s^{-1}$ per standard deviation of OVT). Regressions are calculated separately for each of the 24 models (listed in Table S1) using detrended and deseasonalised monthly means and then averaged (multi-model mean). Dots show regions where the sign of the regression is not the same for all models. Green contours show the zonal wind at 850 hPa (4 and 8 m $s^{-1}$) from the multi-model mean (1850–2005). Black lines show the location of the sections used for calculating the OVT. The dashed box shows the region used to compute the mean zonal wind (U) reported in Table S1.

the volume of water flowing through the ISR is enhanced. Strong winds in the same region and also further downstream have similar effects on the OVT at the BSO (Figure 5b).

To verify if differences in winds are linked to biases in OVT, we calculate the climatological area-averaged zonal wind in the box south of Iceland for every model and compare it to ERA-20C (Table S1). Models with stronger winds south of Iceland (arranged from low to high in Figure 3) are not systematically the models with larger OVT at the ISR. For example, GFDL-ESM2M has a climatological wind lower than MPI-ESM-MR (4.0 vs. 4.4 m $s^{-1}$, respectively) while the mean OVT at the ISR is much higher (9.9 vs. 6.3 Sv, Table S1 and Figure 3c). Likewise, the strength of the climatological wind is also not linked to the climatological OVT at the BSO, and similar conclusions hold when considering wind forcing in a box located further downstream, closer to the BSO, or if other variables (e.g., wind stress curl or mean sea level pressure) are regressed on the OVT (not shown).

## 4. Discussion

In general, from the analyzed models, there is an overall improvement and reduction in the inter-model spread from CMIP5 to CMIP6, especially with respect to temperature (Figure 3). For CMIP5, the inter-model differences in OHT are caused by both OVT and temperature differences, on the contrary to CMIP6 where they are mainly caused by differences in OVT. Since not all models provide OVT for CMIP5 and CMIP6, a direct comparison between the new generation of the same model is possible only for the three pairs IPSL-CM5A-LR/IPSL-CM6A-LR, MPI-ESM-LR/MPI-ESM1-2-LR, NorESM1-M/NorESM2-LM. For both sections, the OVT in the NorESM and MPI-ESM models remain almost unchanged, while it increases considerably and assumes more realistic values in the IPSL-CM6A-LR model (Figure 3). The IPSL-CM5A-LR model has an elevated sea level height in the Arctic, similar to some other CMIP5 models (Richter et al., 2017), and the water is flowing from the Barents Sea toward the Nordic Seas and the North Atlantic (arrows in Figure 1b), leading to negative OVT. The reduced sea level height in the Barents Sea in the IPSL-CM6A-LR model (Figure 1a) leads to an improvement in the representation of the currents, OHT, OVT, and temperatures (see also Boucher et al., 2020).

Some studies have shown that the ocean resolution can improve the OVT, but the improvements might depend on the considered section and model (e.g., Docquier et al., 2020; Heuzé & Årthun, 2019; Olsen et al., 2016). Our results are not straightforward but show that the resolution alone can not explain the inter-model difference in OVT, as models with higher resolution do not have systematically higher or more realistic OVT through both sections (Figure 3).

Observations indicate that the Atlantic Water entering the Barents Sea has warmed over the past decades (Skagseth et al., 2020; Yashayaev & Seidov, 2015). We analyzed temperature only till 2005, but also looked for the considered CMIP6 models at the temperature evolution at the BSO until 2014 (Figure S8). Apart from EC-Earth3, changes in temperature during the last decades are overlaid by large interannual variability.

On multi-annual time scale, OHT correlated well ($r > 0.8$) with both OVT and temperatures at the BSO, in agreement with observations (Orvik & Skagseth, 2005), but less at the ISR, where the correlation between OHT and temperature is low ($r \sim 0.5$, Figure 4c, gray line). To understand the different behaviors at the two sections, we color-coded the correlation between OHT and 100 m temperature based on the correlation values between OVT and 100 m temperature at lag 0 (in red/gray/blue for strong/weak/negative correlations, respectively). At the BSO, most models have high positive correlations between OHT and temperature as well as between OVT and temperature (red triangles, Figure 4d). This might offer an explanation for the good correlations of OHT with both OVT and temperature. At the ISR, however, we observe a large spread in correlations between OHT and temperature, and only a few models show that OVT and temperature anomalies are in phase (few red triangles, Figure 4c). As a result, the multi-model mean correlation between OHT and temperature at the ISR is lower than the one at the BSO. It is still unclear why the models behave so differently, and further studies are needed to clarify it.

The winds south of Iceland and along the Norwegian coast are also important for the OVT variability. When regressing the zonal wind at 850 hPa on OVT at the ISR and BSO, similar patterns emerge in all CMIP models (non-dotted regions in Figure 5), although the strength of the regression varies between models (Figures S6 and S7). This means, for example, that at the BSO a change of one standard deviation of OVT is associated with a change of wind speed

at the BSO of ~0.5 $m\,s^{-1}$ in the GFDL-ESM2G model and of ~1.5 $m\,s^{-1}$ in the GFDL-ESM2M model (Figure S7). Similar results are obtained if the wind is regressed on OHT (Figure S9), as on shorter time scales the OHT reflects the variability in OVT. Winds south of Iceland affect the ocean circulation in terms of barotropic ocean circulation anomalies in the North Atlantic-Nordic Seas exchanges (Sandø et al., 2012), while changes in the strength of the North Atlantic subpolar gyre are mostly responsible for hydrographic anomalies in the inflow region to Nordic Seas (Asbjørnsen et al., 2019; Hátún, Sandø, Drange, Hansen, & Valdimarsson, 2005; Langehaug et al., 2019). The wind regression pattern at the ISR (Figure 5a) resembles the Iceland-Azores dipole of the North Atlantic Oscillation (Woollings et al., 2015), while positive regression values extend further east at the BSO (Figure 5b), indicating that winds along the Norwegian coast are important for OVT into the Barents Sea.

## 5. Conclusion

We analyzed how coupled climate models represent mean and variability of the poleward OHT, as it plays an important role in the energy budget of the Arctic and the sea ice extent therein. Based on the subgroup of CMIP models analyzed here, CMIP6 models have less inter-model spread and OHT mean values closer to observations compared to CMIP5 models, which show biases of several Terawatts at the ISR and BSO (Figure 3). When accounting for decadal variability, at the BSO, CMIP6 models reproduce OHT values comparable to observations and the spread in OHT across CMIP6 models arises mostly from differences in OVT.

OHT variability is strongly controlled by OVT on shorter and longer time scales at both sections (Figure 4). On longer time scales temperature correlations with OHT become as strong as OVT correlations at the BSO, while they are weaker at the ISR, as the variations of OVT and temperature are not necessarily in phase.

Winds south of Iceland and along the Norwegian coast drive much of the OVT variability at the ISR and BSO, respectively (Figure 5). The strength of this link varies across models especially at the BSO, indicating different magnitude in the responses of the ocean circulation to atmospheric forcing. The reason for the differences should be further investigated as they have a direct impact on the OHT variability, which at the BSO is key for the sea ice variability of the Barents Sea (Årthun et al., 2019).

## Data Availability Statement

CMIP data is freely available and was downloaded from https://esgf-node.llnl.gov/search/cmip5/ and https://esgf-node.llnl.gov/search/cmip6/. ERA-20C is available from ECMWF: https://apps.ecmwf.int/datasets/data/era20c-moda/levtype=sfc/type=an/. Timeseries of observed heat, volume transport and temperature were downloaded from the Norwegian Marine Data Centre (NMDC, 2020) https://www.hi.no/hi/forskning/prosjekter/norwegian-marine-data-centre-nmdc, AtlantOS (OceanSITES, 2020) http://www.oceansites.org/tma/index.html and the ICES Report on Ocean Climate (IROC; ICES, 2020) https://ocean.ices.dk/core/iroc.

**Acknowledgments**
We acknowledge the World Climate Research Programme's Working Group on Coupled Modelling, which is responsible for CMIP, and we thank the climate modeling groups (listed in Figure 3) for producing and making available their model output. For CMIP the U.S. Department of Energy's Program for Climate Model Diagnosis and Intercomparison provides coordinating support and led development of software infrastructure in partnership with the Global Organization for Earth System Science Portals. Part of this work was funded by the Research Council of Norway through the project The Nansen Legacy (RCN 276 730) and by basic institutional support from the Norwegian Department of Education to the Bjerknes Centre for Climate Research (EMULATE). We also acknowledge storage space from the Norwegian National e-Infrastructure for Research Data (NIRD, NS9252K) and Camille Li, Aleksi Nummelin, Øystein Skagseth, Stefan Sobolowski and Marius Årthun for fruitful discussions. We thank two anonymous reviewers for their comments, which helped improving the manuscript.

## References

ACIA, Arctic Climate Impact Assessment. (2004). *Impacts of a warming Arctic-Arctic climate impact assessment* (p. 144). Cambridge University Press.

Årthun, M., Eldevik, T., Smedsrud, L., Skagseth, Ø., & Ingvaldsen, R. (2012). Quantifying the influence of Atlantic heat on Barents Sea ice variability and retreat. *Journal of Climate*, *25*(13), 4736–4743. https://doi.org/10.1175/jcli-d-11-00466.1

Årthun, M., Eldevik, T., & Smedsrud, L. H. (2019). The role of Atlantic heat transport in future Arctic winter sea ice loss. *Journal of Climate*, *32*(11), 3327–3341. https://doi.org/10.1175/jcli-d-18-0750.1

Asbjørnsen, H., Årthun, M., Skagseth, Ø., & Eldevik, T. (2019). Mechanisms of ocean heat anomalies in the Norwegian Sea. *Journal of Geophysical Research: Oceans*, *124*(4), 2908–2923.

Berx, B., Hansen, B., Østerhus, S., Larsen, K., Sherwin, T., & Jochumsen, K. (2013). Combining in-situ measurements and altimetry to estimate volume, heat and salt transport variability through the Faroe Shetland Channel. *Ocean Science Discussions*, *10*(1). https://doi.org/10.5194/os-9-639-2013

Boccaletti, G., Ferrari, R., Adcroft, A., Ferreira, D., & Marshall, J. (2005). The vertical structure of ocean heat transport. *Geophysical Research Letters*, *32*(10). https://doi.org/10.1029/2005gl022474

Boucher, O., Servonnat, J., Albright, A. L., Aumont, O., Balkanski, Y., Bastrikov, V., et al. (2020). Presentation and evaluation of the IPSL-CM6A-LR climate model. *Journal of Advances in Modeling Earth Systems*, *12*(7), 1–52.

Buckley, M. W., & Marshall, J. (2016). Observations, inferences, and mechanisms of the Atlantic Meridional overturning circulation: A review. *Reviews of Geophysics*, *54*(1), 5–63. https://doi.org/10.1002/2015rg000493

Burgard, C., & Notz, D. (2017). Drivers of Arctic Ocean warming in CMIP5 models. *Geophysical Research Letters*, *44*(9), 4263–4271. https://doi.org/10.1002/2016gl072342

Chelton, D. B. (1983). Effects of sampling errors in statistical estimation. *Journal of Physical Oceanography*. *30*(103). https://doi.org/10.1016/0198-0149(83)90062-6

Cinquini, L., Crichton, D., Mattmann, C., Harney, J., Shipman, G., Wang, F., et al. (2014). The Earth System Grid Federation: An open infrastructure for access to distributed geospatial data. *Future Generation Computer Systems*, *36*, 400–417. https://doi.org/10.1016/j.future.2013.07.002

Davy, R., & Outten, S. (2020). The Arctic surface climate in CMIP6: Status and developments since CMIP5. *Journal of Climate*, *33*(18), 8047–8068. https://doi.org/10.1175/jcli-d-19-0990.1

Docquier, D., Fuentes-Franco, R., Koenigk, T., & Fichefet, T. (2020). Sea ice—Ocean interactions in the Barents Sea modeled at different resolutions. *Frontiers of Earth Science*, *8*, 172. https://doi.org/10.3389/feart.2020.00172

Docquier, D., Koenigk, T., Fuentes-Franco, R., Karami, M. P., & Ruprich-Robert, Y. (2021). Impact of ocean heat transport on the Arctic sea-ice decline: A model study with EC-Earth3. *Climate Dynamics*, 1–26. https://doi.org/10.1007/s00382-020-05540-8

Eyring, V., Bony, S., Meehl, G. A., Senior, C. A., Stevens, B., Stouffer, R. J., & Taylor, K. E. (2016). Overview of the Coupled Model Intercomparison Project Phase 6 (CMIP6) experimental design and organization. *Geoscientific Model Development*, *9*(5), 1937–1958. https://doi.org/10.5194/gmd-9-1937-2016

Hansen, B., & Østerhus, S. (2000). North Atlantic–Nordic Seas exchanges. *Progress in Oceanography*, *45*(2), 109–208. https://doi.org/10.1016/s0079-6611(99)00052-x

Hansen, B., & Østerhus, S. (2007). Faroe bank channel overflow 1995–2005. *Progress in Oceanography*, *75*(4), 817–856. https://doi.org/10.1016/j.pocean.2007.09.004

Harvey, B., Cook, P., Shaffrey, L., & Schiemann, R. (2020). The response of the Northern Hemisphere storm tracks and jet streams to climate change in the CMIP3, CMIP5, and CMIP6 climate models. *Journal of Geophysical Research: Atmospheres*, e2020JD032701. https://doi.org/10.1029/2020jd032701

Hátún, H., Sandø, A. B., Drange, H., & Bentsen, M. (2005). Seasonal to decadal temperature variations in the Faroe-Shetland inflow waters. In H. Drange, T. Dokken, T. Furevik, R. Gerdes, & W. Berger (Eds.), *The Nordic Seas: An integrated perspective* (pp. 239–250). American Geophysical Union. https://doi.org/10.1029/158gm16

Hátún, H., Sandø, A. B., Drange, H., Hansen, B., & Valdimarsson, H. (2005). Influence of the Atlantic subpolar gyre on the thermohaline circulation. *Science*, *309*(5742), 1841–1844.

Heuzé, C., & Årthun, M. (2019). The Atlantic inflow across the Greenland-Scotland ridge in global climate models (CMIP5). *Elementa: Science of the Anthropocene.*, *7*(1), 16. https://doi.org/10.1525/elementa.354

Huang, Y., Xia, Y., & Tan, X. (2017). On the pattern of $CO_2$ radiative forcing and poleward energy transport. *Journal of Geophysical Research: Atmospheres*, *122*(20), 10–578. https://doi.org/10.1002/2017jd027221

ICES. (2020). *ICES Report on ocean climate*. Retrieved from https://ocean.ices.dk/core/iroc. Accessed on 2020-06-30.

Ikeda, M. (1990). Decadal oscillations of the air-ice-ocean system in the Northern Hemisphere. *Atmosphere-Ocean*, *28*(1), 106–139. https://doi.org/10.1080/07055900.1990.9649369

Ingvaldsen, R. B., Asplin, L., & Loeng, H. (2004). The seasonal cycle in the Atlantic transport to the Barents Sea during the years 1997–2001. *Continental Shelf Research*, *24*(9), 1015–1032. https://doi.org/10.1016/j.csr.2004.02.011

Langehaug, H. R., Sandø, A. B., Årthun, M., & Ilıcak, M. (2019). Variability along the Atlantic water pathway in the forced Norwegian earth system model. *Climate Dynamics*, *52*(1), 1211–1230. https://doi.org/10.1007/s00382-018-4184-5

Li, D., Zhang, R., & Knutson, T. R. (2017). On the discrepancy between observed and CMIP5 multi-model simulated Barents Sea winter sea ice decline. *Nature Communications*, *8*(1), 1–7. https://doi.org/10.1038/ncomms14991

Lien, V. S., Schlichtholz, P., Skagseth, Ø., & Vikebø, F. B. (2017). Wind-driven Atlantic water flow as a direct mode for reduced Barents Sea ice cover. *Journal of Climate*, *30*(2), 803–812. https://doi.org/10.1175/jcli-d-16-0025.1

Muilwijk, M., Ilicak, M., Cornish, S. B., Danilov, S., Gelderloos, R., Gerdes, R., et al. (2019). Arctic Ocean response to Greenland Sea wind anomalies in a suite of model simulations. *Journal of Geophysical Research: Oceans*, *124*(8), 6286–6322. https://doi.org/10.1029/2019jc015101

Muilwijk, M., Smedsrud, L. H., Ilicak, M., & Drange, H. (2018). Atlantic Water heat transport variability in the 20th century Arctic Ocean from a global ocean model and observations. *Journal of Geophysical Research: Oceans*, *123*(11), 8159–8179. https://doi.org/10.1029/2018jc014327

NMDC. (2020). *Norwegian Marine Data Centre*. Retrieved from https://www.hi.no/hi/forskning/prosjekter/norwegian-marine-data-centre-nmdc, Accessed on 2020-06-30.

Notz & SIMIP Community. (2020). Arctic sea ice in CMIP6. *Geophysical Research Letters*, *47*(10), e2019GL086749. https://doi.org/10.1029/2019gl086749

Nummelin, A., Li, C., & Hezel, P. J. (2017). Connecting ocean heat transport changes from the midlatitudes to the Arctic ocean. *Geophysical Research Letters*, *44*(4), 1899–1908. https://doi.org/10.1002/2016gl071333

OceanSITES. (2020). *Optimising and Enhancing the Integrated Atlantic Ocean Observing Systems*, AtlantOS. Retrieved from http://www.oceansites.org/tma/index.html. Accessed on 2020-06-30.

Olsen, S., Hansen, B., Østerhus, S., Quadfasel, D., & Valdimarsson, H. (2016). Biased thermohaline exchanges with the Arctic across the Iceland–Faroe Ridge in ocean climate models. *Ocean Science*, *12*(2), 545–560. https://doi.org/10.5194/os-12-545-2016

Onarheim, I. H., Eldevik, T., Årthun, M., Ingvaldsen, R. B., & Smedsrud, L. H. (2015). Skillful prediction of Barents Sea ice cover. *Geophysical Research Letters*, *42*(13), 5364–5371. https://doi.org/10.1002/2015gl064359

Orvik, K. A., & Skagseth, Ø. (2003). The impact of the wind stress curl in the North Atlantic on the Atlantic inflow to the Norwegian Sea toward the Arctic. *Geophysical Research Letters*, *30*(17). https://doi.org/10.1029/2003gl017932

Orvik, K. A., & Skagseth, Ø. (2005). Heat flux variations in the eastern Norwegian Atlantic Current toward the Arctic from moored instruments. *Geophysical Research Letters*, *32*(14). https://doi.org/10.1029/2005gl023487

Oudar, T., Cattiaux, J., & Douville, H. (2020). Drivers of the northern extratropical eddy-driven jet change in CMIP5 and CMIP6 models. *Geophysical Research Letters*, *47*(8), e2019GL086695. https://doi.org/10.1029/2019gl086695

Poli, P., Hersbach, H., Dee, D. P., Berrisford, P., Simmons, A. J., Vitart, F., et al. (2016). ERA-20C: An atmospheric reanalysis of the twentieth century. *Journal of Climate*, *29*(11), 4083–4097.

Priestley, M. D., Ackerley, D., Catto, J. L., Hodges, K. I., McDonald, R. E., & Lee, R. W. (2020). An overview of the extratropical storm tracks in CMIP6 historical simulations. *Journal of Climate*. https://doi.org/10.1175/jcli-d-19-0928.1

Richter, K., Furevik, T., & Orvik, K. (2009). Effect of wintertime low-pressure systems on the Atlantic inflow to the Nordic seas. *Journal of Geophysical Research: Oceans*, *114*(C9). https://doi.org/10.1029/2009jc005392

Richter, K., Øie Nilsen, J. E., Raj, R. P., Bethke, I., Johannessen, J. A., Slangen, A. B., & Marzeion, B. (2017). Northern North Atlantic Sea level in CMIP5 climate models: Evaluation of mean state, variability, and trends against altimetric observations. *Journal of Climate*, *30*(23), 9383–9398. https://doi.org/10.1175/jcli-d-17-0310.1

Sandø, A. B., & Furevik, T. (2008). Relation between the wind stress curl in the North Atlantic and the Atlantic inflow to the Nordic Seas. *Journal of Geophysical Research: Oceans*, *113*(C6). https://doi.org/10.1029/2007JC004236

Sandø, A. B., Gao, Y., & Langehaug, H. R. (2014). Poleward ocean heat transports, sea ice processes, and Arctic sea ice variability in NorESM1-M simulations. *Journal of Geophysical Research: Oceans*, *119*(3), 2095–2108.

Sandø, A. B., Nilsen, J. E., Eldevik, T., & Bentsen, M. (2012). Mechanisms for variable North Atlantic–Nordic Seas exchanges. *Journal of Geophysical Research: Oceans*, *117*(C12).

Screen, J. A., & Simmonds, I. (2010). The central role of diminishing sea ice in recent Arctic temperature amplification. *Nature*, *464*(7293), 1334–1337. https://doi.org/10.1038/nature09051

Serra, N., Kaese, R. H., Kähl, A., Stammer, D., & Quadfasel, D. (2010). On the low-frequency phase relation between the Denmark Strait and the Faroe-Bank Channel overflows. *Tellus A: Dynamic Meteorology and Oceanography*, *62*(4), 530–550. https://doi.org/10.1111/j.1600-0870.2010.00445.x

Serreze, M. C., Barrett, A. P., Stroeve, J. C., Kindig, D. N., & Holland, M. M. (2009). The emergence of surface-based Arctic amplification. *The Cryosphere*, *3*(1), 11, 19. https://doi.org/10.5194/tc-3-11-2009

Serreze, M. C., & Barry, R. G. (2011). Processes and impacts of Arctic amplification: A research synthesis. *Global and Planetary Change*, *77*(1), 85 – 96. https://doi.org/10.1016/j.gloplacha.2011.03.004

Skagseth, Ø. (2008). Recirculation of Atlantic water in the western Barents Sea. *Geophysical Research Letters*, *35*(11), L11606. https://doi.org/10.1029/2008GL033785

Skagseth, Ø., Drinkwater, K. F., & Terrile, E. (2011). Wind-induced transport of the Norwegian Coastal Current in the Barents Sea. *Journal of Geophysical Research: Oceans*, *116*(C08007), 1–15. https://doi.org/10.1029/2011JC006996

Skagseth, Ø., Eldevik, T., Årthun, M., Asbjørnsen, H., Lien, V. S., & Smedsrud, L. H. (2020). Reduced efficiency of the Barents Sea cooling machine. *Nature Climate Change*, *10*(7), 661–666. https://doi.org/10.1038/s41558-020-0772-6

Skagseth, Ø., Furevik, T., Ingvaldsen, R., Loeng, H., Mork, K. A., Orvik, K. A., & Ozhigin, V. (2008). Volume and heat transports to the Arctic Ocean via the Norwegian and Barents Seas. In *Arctic–Subarctic Ocean fluxes* (pp. 45–64). https://doi.org/10.1007/978-1-4020-6774-7_3

Smedsrud, L. H., Esau, I., Ingvaldsen, R. B., Eldevik, T., Haugan, P. M., Li, C., et al.(2013). The role of the Barents Sea in the Arctic climate system. *Reviews of Geophysics*, *51*(3), 415–449. https://doi.org/10.1002/rog.20017

Spielhagen, R. F., Werner, K., Sørensen, S. A., Zamelczyk, K., Kandiano, E., Budeus, G., et al. (2011). Enhanced modern heat transfer to the Arctic by warm Atlantic water. *Science*, *331*(6016), 450–453. https://doi.org/10.1126/science.1197397

Stroeve, J. C., Kattsov, V., Barrett, A., Serreze, M., Pavlova, T., Holland, M., & Meier, W. N. (2012). Trends in Arctic sea ice extent from CMIP5, CMIP3 and observations. *Geophysical Research Letters*, *39*(16). https://doi.org/10.1029/2012gl052676

Taylor, K. E., Stouffer, R. J., & Meehl, G. A. (2012). An overview of CMIP5 and the experiment design. *Bulletin of the American Meteorological Society*, *93*(4), 485–498. https://doi.org/10.1175/bams-d-11-00094.1

Winton, M. (2006). Amplified arctic climate change: What does surface albedo feedback have to do with it? *Geophysical Research Letters*, *33*(3). https://doi.org/10.1029/2005gl025244

Woollings, T., Franzke, C., Hodson, D., Dong, B., Barnes, E. A., Raible, C., & Pinto, J. (2015). Contrasting interannual and multidecadal NAO variability. *Climate Dynamics*, *45*(1–2), 539–556. https://doi.org/10.1007/s00382-014-2237-y

Yashayaev, I., & Seidov, D. (2015). The role of the Atlantic Water in multidecadal ocean variability in the Nordic and Barents Seas. *Progress in Oceanography*, *132*, 68–127. https://doi.org/10.1016/j.pocean.2014.11.009

Zappa, G., Masato, G., Shaffrey, L., Woollings, T., & Hodges, K. (2014). Linking Northern Hemisphere blocking and storm track biases in the CMIP5 climate models. *Geophysical Research Letters*, *41*(1), 135–139. https://doi.org/10.1002/2013gl058480